Science and Innovation of Advanced Materials

The Materials Research Society of Thailand

Research Article

Co-doped Rutile-TiO_2 Ceramics: Promising Giant Dielectric Oxides

Wattana Tuichai[1], Jakkree Boonlakhorn[1], Pornjuk Srepusharawoot[1], Prasit Thongbai[1,*], Bundit Putasaeng[2], Supamas Danwittayakul[2], Worawat Meevasana[1], Santi Maensiri[3]

[1] Giant Dielectric and Computational Design Research Group (GD–CDR), Department of Physics, Faculty of Science, Khon Kaen University, Khon Kaen 40002, Thailand
[2] National Metal and Materials Technology Center, National Science and Technology Development Agency, Thailand Science Park, Pathum Thani 12120, Thailand
[3] School of Physics, Institute of Science, Suranaree University of Technology, Nakhon Ratchasima 30000, Thailand

* Corresponding author e-mail: pthongbai@kku.ac.th

Received: *January 23th, 2022* | ***Revised:*** *July 13th, 2022* | ***Accepted:*** *July 13th, 2022*

Abstract: Recently, many kinds of dielectric materials have been intensively reported to display giant (or colossal) dielectric permittivity (GDP) > 10^4 at room temperature in the radio-frequency range. Improvement and modification of GDP have been performed to obtain significantly improved GDP performance for promising applications, such as ceramic capacitors, modern electronics, sensors, and multifunctional devices. In this paper, a short review of various GDP materials is represented based on the interfacial polarization at internal interfaces. An argument between the intrinsic and extrinsic factors on the GDP behavior is discussed. Then, the formation of Schottky barriers at the internal interfaces that can give rise to the appearance of the GDP is briefly reviewed. Finally, co-doped rutile-TiO_2 systems are demonstrated to be an exciting GDP material. Low dielectric loss tangent (< 0.025) and giant dielectric permittivity of 10^4 with nearly temperature-independent over the temperature range of -55 – 200 °C. A newly reported model, i.e., an electron-pinned defect-dipole model, is proposed to be the primary contribution of the co-doped TiO_2 materials.

Keywords: Giant/Colossal dielectric properties, Impedance spectroscopy, IBLC, SBLC, Electron-pinned defect-dipoles

1. Giant dielectric oxides from the past to the future

1.1 Dielectric oxides and their potential applications

Dielectric materials with ultra-high dielectric constants ($\varepsilon' > 10^4$), also known as "*a giant or colossal dielectric permittivity (GDP) material*", have attracted considerable attention due to their high potential for applications in modern technologies such as energy storage, modern electronics, sensors, and multifunctional devices, especially in electronic devices such as multilayer ceramic capacitors (MLCCs) [1-6]. As a result of technological progress in modern communication technology and microelectronics, investigation and development of new types of GDP materials have been intensively pursued [1-5,7-25]. In recent years, the discovery of dielectric oxides exhibiting ultra-high ε' and low

loss tangent (tanδ) further stimulated research activity [2,7,10,12]. Generally, the ε′ values of a dielectric that was selected as capacitive layers are the major factor determining the performance of MLCC [1]. The dimension of MLCCs can be reduced by using dielectric layers with a dielectric having a relatively high ε′. Furthermore, for many applications, the ε′ value must be high to increase the volumetric efficiency of the MLCC [4]. Tanδ, the temperature stability of ε′, DC voltage dependence of ε′, and the resistivity of dielectric are also important parameters [26]. Tanδ must be reduced to avoid draining the stored charge, and to decrease the dissipation of stored energy into heat. The capacitance should have excellent temperature stability so that the capacitor will operate properly over a wide temperature range. If the temperature dependence of ε′ of dielectric layers is large, the device will not be robust [2].

For class II and III ceramic capacitors, tanδ of dielectrics at 25 °C and 1 kHz must be lower than 0.025 and 0.040, respectively [26]. The value of ε′ should be larger than 10^3 (at 1 kHz and 25 °C) or as high as possible. This is needed to support new technologies requiring low-weight electronic devices. In MLCCs, the temperature coefficient of capacitance (or temperature coefficient of ε′, Δε′ (%)) of a dielectric is the critical factor. For an X7R capacitor, Δε′ (%) or $\Delta C/C_{25}$ (%) (compared to the ε′ value at 1 kHz and 25 °C) of a dielectric that was selected to produce this type of capacitor must be ≤ ±15% in the temperature range of -55 – 125 °C [26]. This is necessary to obtain the temperature dependence of capacitance that varies ≤ ±15% in this temperature range. For X8R and X9R capacitors, Δε′ (%) must be ≤ ±15% in the temperature ranges of -55 – 150 °C and -55 – 200 °C, respectively [26]. The demand for electronic components that can be operated at high temperatures has dramatically increased due to the rapid development of new technologies. Therefore, the capacitance of a capacitor must slightly change as temperature increases. This can be obtained by using a dielectric material with a ε′ that is stable over a wide temperature range. High ε′ values, 10^3 – 10^4, are usually exhibited by $BaTiO_3$–based ceramics [11,26]. Unfortunately, their ε′ values are significantly temperature-dependent, and thus ferroelectric MLCCs might be hampered by considering their temperature stability [11].

1.2 Giant dielectric oxides

Recently, a large number of classic GDP materials with very large ε′ values (> 10^4 at room temperature and in the radio-frequency range) have been reported. They are considered potentially useful capacitor materials. These GDP materials are $CaCu_3Ti_4O_{12}$ and related compounds [1,7-9,13,27-41], CuO [10,42,43], $Ln_{2-x}Sr_xNiO_4$ (*Ln* = Nd, La, Sm) [11,12,44-50], (*M*,*N*)-doped NiO systems (*M* = Li, Na, K and *N* = Ti, Al, Si, Ta) [2,51-56], $AFe_{1/2}B_{1/2}O_3$ (**A** = Ba, Sr, Ca; **B** = Nb, Ta, Sb) [14,57-59], and $LuFe_2O_4$ [60] ceramics as well as $BaTiO_3$/Ni composite materials [61]. Unfortunately, tanδ values of these GDP oxides are larger than the standard values for capacitor applications. Tanδ values of these materials are still larger than 0.1 at 1 kHz. This is a serious problem that hinders the practical applications of these materials. Many researchers believe that the large tanδ values of these materials are the most serious problem. However, to the best of our knowledge, the temperature stability of ε′ (Δε′ (%)) is more a serious and difficult problem to solve [62]. For example, $CaCu_3Ti_4O_{12}$ ceramics are giant-dielectric materials that have been most actively studied in recent years. Large reduction of tanδ (tanδ < 0.04) was successfully achieved by several methods [62-66]. However, a strong reduction of tanδ is usually accompanied by a large decrease in ε′ [66]. Furthermore, most research found that the temperature stability that meets the condition of Δε′ (%) < ±15% was accomplished at temperatures below 100 °C [62,64,67,68]. Large increases in ε′ at high temperatures are usually due to DC conduction in materials and the electrical response of grain boundaries.

Among these GDP materials, $Ln_{2-x}Sr_xNiO_4$ (*Ln* = Nd, La, Sm) ceramics are most interesting. This results from three factors. First, these ceramics can exhibit very high ε′ values of 10^5 – 10^6 [4,11]. ε′ values of this material system are the largest compared to other materials. Second, such high ε′ is observed at relatively high frequencies, in the range of 10^9 Hz (GHz region) [11]. This has never been observed in other giant dielectric materials. Third, by considering materials science coupled with the resource strategy and resource management as proposed by Krohns and co-workers serve as guidelines for the development of novel materials. $La_{2-x}Sr_xNiO_4$ ceramic (LSNO) has been judged potentially more important in the future compared to $BaTiO_3$ and $CaCu_3Ti_4O_{12}$ ceramics [4]. Tanδ value of $La_{2-x}Sr_xNiO_4$ ceramics is the only one factor that has to be lowered. Therefore, it is wise to investigate to reduce the tanδ values of

$La_{2-x}Sr_xNiO_4$ ceramics. High value ε' and tanδ of the $La_{2-x}Sr_xNiO_4$ ceramic originate from charge ordering due to a small polaronic hopping process [12,46-48]. Delocalized charges are the primary cause of DC conduction in ceramics, resulting in a high tanδ value [69]. Reduction of tanδ may be achieved by creating localized charges in designated lattice defect states and/or increasing the resistance of grain boundaries [3,8,62]. Thus, the investigation on the strategy to greatly reduce tanδ of the $La_{2-x}Sr_xNiO_4$ ceramic system is an important topic to seek a novel GDP material.

Most recently, Hu et al. (2013) [3] reported a novel GDP (GDP) oxide with fascinating dielectric properties in the rutile-TiO_2 ceramics co-doped with In^{3+}/Nb^{5+} ions. Ceramic with composition of $(In_{0.05}Nb_{0.05})_xTi_{1-x}O_2$ where x = 0.1 exhibited a high ε' (~6×10^4) with tanδ ~0.02 over a frequency range of $10^2 - 10^6$ Hz. Furthermore, the temperature stability of ε' was achieved in the temperature range of 80 – 450 K was accomplished. These interesting GDP properties are reasonably explained by the formation of large defect-dipole clusters. The defects contained largely localized electrons. Partial substitution of rutile-TiO_2 ceramic by Nb^{5+} ions created free electrons by reducing Ti^{4+} to Ti^{3+}. In contrast, the substitution of In^{3+} into rutile-TiO_2 ceramic has a slight influence on the dielectric response but resulted in the reduction in dielectric losses at higher frequencies. According to the nominal composition of $(In_{0.05}Nb_{0.05})_xTi_{1-x}O_2$, the complex stoichiometry of $(In_x^{3+}Nb_x^{5+}Ti_x^{3+})Ti_{1-3x}^{4+}O_{2-x/2}$ produces defect clusters, where the electrons created by both Nb^{5+} doping and the reduction of Ti^{4+} to Ti^{3+} are contained by the presence of In^{3+} [5]. Without the latter, electrons would delocalize and lead to high tanδ. This is a new model that was proposed as the origin of the giant dielectric response in oxides. Excellent-dielectric performance can be created by engineering the local structure within the structure of rutile-TiO_2.

Finally, for new generation electronic technologies, flexible electronic devices have been intensively developed and in progress. Flexible polymeric dielectric materials have attracted attention because of their ease of processing, flexibility, and ultra-high breakdown voltage [70-74]. Polyvinylidene fluoride (PVDF) will be used as a matrix since it has the highest ε' among polymer-dielectric materials [75-77]. However, the ε' value of these polymers is very low compared to those of many ceramics. Recently, polymer-ceramic composites were widely investigated to enhance the value of ε' in dielectric-polymer materials. However, ε' of polymer-ceramic (i.e., $BaTiO_3$) composites still remains low level (~50) at room temperature [74]. High-ε' values (60-500) were reported in polymer-ceramic composites using giant dielectric materials as fillers. These include $CaCu_3Ti_4O_{12}$, (Li, Ti)-doped NiO, and CuO [77-80].

1.3 Comparison of dielectric oxides

Many GDP material groups have been intensively investigated. GDP material groups and high-permittivity dielectric materials consist of $CaCu_3Ti_4O_{12}$ and related compounds [1,7-9,28-31,64-66], CuO [10,42,43], $\boldsymbol{Ln}_{2-x}Sr_xNiO_4$ ($\boldsymbol{Ln}$ = Nd, La, Sm) [11,12,44,46-48], ($\boldsymbol{M}$,$\boldsymbol{N}$)-doped NiO systems ($\boldsymbol{M}$ = Li, Na, K and $\boldsymbol{N}$ = Ti, Al, Si, Ta) [2,51-54,56], $\mathbf{A}Fe_{1/2}\mathbf{B}_{1/2}O_3$ ($\mathbf{A}$ = Ba, Sr, Ca; $\mathbf{B}$ = Nb, Ta, Sb) [14,57-59], $TbMnO_3$ [81], (In+Nb)-doped TiO_2 [3,5,82], $Ni_{0.5}Zn_{0.5}FeO_2$ [83], and $LuFe_2O_4$ [60] ceramics as well as $BaTiO_3$/Ni composite materials [61]. Most of these materials exhibit similar dielectric behavior with the exception for $La_{2-x}Sr_xNiO_4$ ceramics. These giant-dielectric materials exhibit high ε' values of ($10^4 - 10^5$) at room temperature at frequencies below 10^6 Hz. In contrast, a high ε' value (~10^4) of $La_{2-x}Sr_xNiO_4$ ceramics can be observed in the GHz region (10^9 Hz), while ε' values in the radio frequency range were found to be $10^5 - 10^6$. The dielectric parameters of these materials at different conditions are summarized in Table 1.

Although $CaCu_3Ti_4O_{12}$ are the mostly studied giant-dielectric materials since their discovery by Subramanian and co-workers [7], low-temperature stability of ε' is still the most serious problem. High tanδ remains a major problem. When the temperature was increased to more than 100 °C, ε' increased dramatically [62,64,68]. The improved dielectric properties of $CaCu_3Ti_4O_{12}$ were achieved in Yb-doped $CaCu_3Ti_4O_{12}$ ceramics with ε' ~1.6×10^4 and tanδ ~0.015 as well as $\Delta\varepsilon'$ (%) < ±15% at temperatures below 130 °C [62]. Considering applications in a GHz frequency range, $CaCu_3Ti_4O_{12}$ fails. Its giant-dielectric behavior disappears in this region. As shown in Table 1, the dielectric properties of $BaTiO_3$/Ni composites are fascinating. High ε' and low tanδ values were observed in this ceramic-metal composite system. However, the method to obtain this composite material is very complex [61]. Sintering in a reducing atmosphere must be done with extreme care. This is not practical for commercial applications.

Table 1 Dielectric properties of several giant-dielectric material groups at room temperature

Materials	$f = 10^3$ Hz		$f = 10^6 - 10^9$ Hz		References
	ε′	tanδ	ε′	tanδ	
$CaCu_3Ti_4O_{12}$	~$10^3 - 10^5$	> 0.1	~10^2	-	[1,7-9,31]
$Na_{1/2}Bi_{1/2}Cu_3Ti_4O_{12}$	~10^4	> 0.1	~2.5×10^2	-	[13,84]
(Li,Ti)-doped NiO	~$10^4 - 10^5$	> 0.4	~3.0×10^2	-	[2]
CuO	~10^4	20	~2.0×10^2	-	[10,42]
$LuFe_2O_4$	0.48×10^4	-	~10^2	-	[60]
$BaTiO_3$/Ni	8.0×10^4	0.05	-	-	[61]
$AFe_{1/2}B_{1/2}O_3$	~$10^3 - 10^5$	> 0.1	~10^2	-	[14,57-59]
$TbMnO_3$	~10^4	> 4.0	~10^2	-	[81]
$Ni_{0.5}Zn_{0.5}FeO_2$	~10^5	> 1.0	< 10^2	-	[83]
$La_{15/8}Sr_{1/8}NiO_4$	~$10^4 - 10^5$	> 10	~10^4	~0.1	[11]
(In+Nb)-doped TiO_2	~6.0×10^4	< 0.02	~10^4	> 0.1	[3]
$BaTiO_3$-based ceramics	~$10^3 - 10^4$	< 0.02	~10^3	-	[4]

1.4 Origins of giant dielectric properties: Extrinsic effects vs. quasi-intrinsic effect

Recently, ceramic oxides exhibiting a so-called "*giant dielectric permittivity*" or "*colossal dielectric permittivity*" (ε′) have been reported in both of simple and complex oxides [2,3,10,85-90]. Because of the initial excitement of the discovery of possible "novel" intrinsic polarization mechanisms, which were associated either with an electronic charge ordering or unusual crystal structure. It is widely demonstrated in many oxides that the giant dielectric-permittivity effect is often associated with a well-known extrinsic Maxwell–Wagner-type polarization, which is not related to an intrinsic property [85,91-93]. Schottky barriers can be formed in electrically heterogeneous semiconductors and are often the origin of an interfacial Maxwell–Wagner polarization when applied electric field. This results in the observation of tremendous values of capacitance (≈0.1 – 10 nF cm^{-1}), especially when measured at the radio-frequency range, giving rise to artifacts of high dielectric response in semiconducting materials such as single crystalline $CaCu_3Ti_4O_{12}$ (CCTO) and (In+Nb) co-doped TiO_2 (INTO) ceramics [1,94]. There are at least three types of strong polarization artifacts related to the formation of Schottky barriers, i.e., a Schottky barrier at the interface between semiconducting grains (grain boundary), the interface between resistive outer-surface layer, and semiconducting inner core, and the interface between the metal electrode and semiconducting sample surface. All cases can cause apparent very high dielectric permittivity.

1.4.1 Extrinsic effects

- Internal barrier layer capacitor (IBLC) effect

As shown in Figure 1, this effect is owing to the formation of Schottky barriers between semiconducting grains and resistive grain boundaries in ceramics [91]. The related high effective dielectric-permittivity, ε'_{eff}, where $\varepsilon'_{eff} = C/\varepsilon_0$ and $\varepsilon_0 = 8.854 \times 10^{-14}$ F cm^{-1}, has a close relationship to the microstructure, which can be roughly estimated using the expression $\varepsilon'_{eff} = \varepsilon'_r(S/t_{gb})$ [2,95], where ε'_r is the dielectric permittivity of the grain boundary and assumed to be the same as that of the bulk response; S and t_{gb} are the average grain size and thickness of the grain boundary, respectively. Although the IBLC model is a very simplified approximation, the above expression can give a reasonable evaluation of ε'_{eff} in IBLC-type ceramics for many cases. The dielectric permittivity or measured capacitance value increases with increasing the mean grain size, while the tanδ decreased [85]. The decrease in tanδ in the large-grained

CCTO ceramic is usually due to the decrease in the number of the insulating grain boundary layer. Based on the IBLC structural model, the tanδ is inversely proportional to R_{gb} following to the equation [69,96]:

$$\tan\delta \approx \frac{1}{\omega\varepsilon_0\varepsilon_s' C_0 R_{gb}} \quad , \qquad (1)$$

where ε_s' is the dielectric permittivity over a low-frequency range. C_o is the empty cell capacitance. R_{gb} decreases with increasing the mean grain size, resulting in an increase in a low-frequency tanδ value.

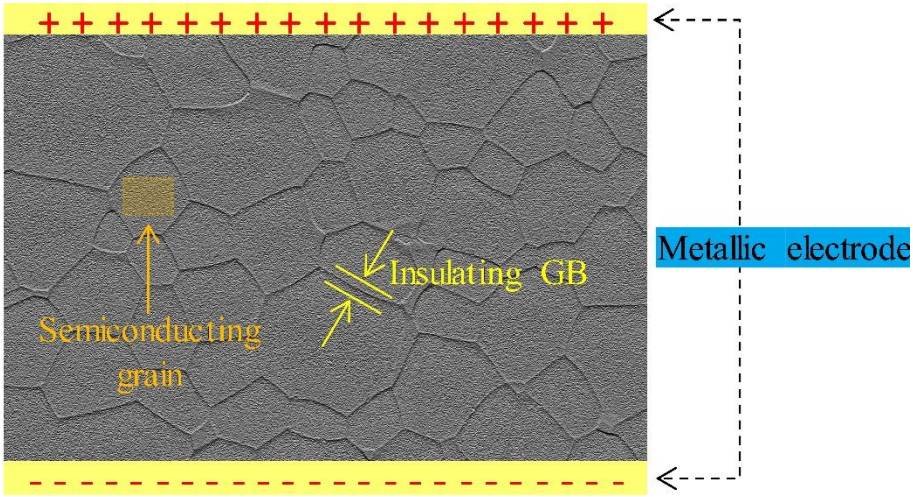

Figure 1 IBLC structure consisting of semiconducting grains and insulating grain boundaries.

- Surface barrier layer capacitor (SBLC) effect

The second kind of Schottky barrier can be produced at the interface between a resistive outer-surface skin layer and a semiconducting inner core of a sintered sample, as shown in Figure 2. This surface barrier layer capacitor (SBLC) effect is deliberately in $(Ba_{1-x}Sr_x)TiO_{3-\delta}$ (BSTO), where δ is a small level of oxygen deficiency [26,85,97]. When BSTO is sintered in a reducing atmosphere, the annealed BSTO ceramics contains d^0 cations (e.g., Ti^{4+} and Nb^{5+}). These ions become partially reduced to be Ti^{3+} and Nb^{4+}, respectively. In this stage, the BSTO ceramics become oxygen-deficient and exhibit semiconductivity. Annealing the BSTO ceramics in an oxygen atmosphere at temperatures lower than sintering leads to limited re-oxidation at the sample surfaces. Eventually, a resistive outer surface layer is formed, with the center of the sample remaining reduced and semiconducting. Although this phenomenon can be used to deliberately generate electrically heterogeneous ceramics exhibiting very high effective permittivity, such BSTO ceramics simultaneously exhibit high tanδ dielectric loss. This is the primary limitation in many technological applications. This SBLC effect can also be reported in CCTO and NiO-based ceramics [98,99]. However, the tanδ of a CCTO ceramic with a resistive outer surface layer is still too large (> 1.0 at 300 K).

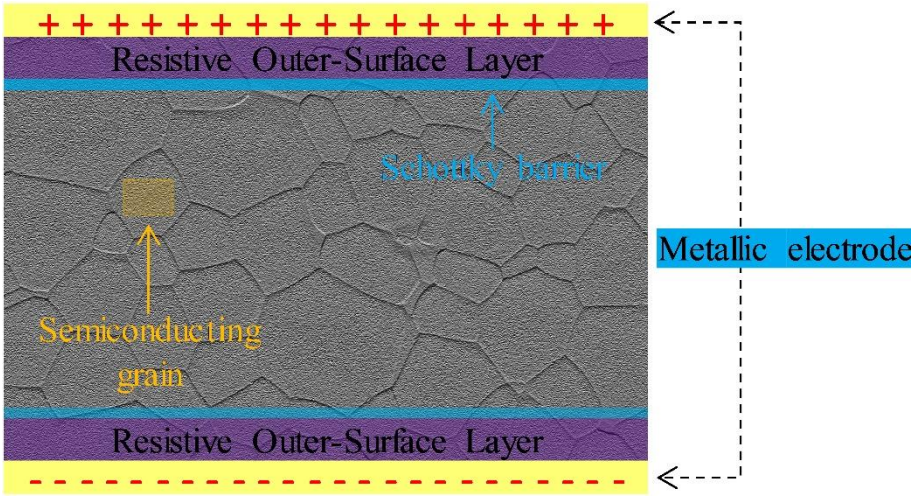

Figure 2 SBLC structure consisting of semiconducting core and insulative outer surface layers.

- Sample-electrode interface (S-E) effect

Finally, another commonly observed artifact, referred to as an electrode effect, is associated with the formation of Schottky barriers between a semiconducting sample surface and metal electrodes, as demonstrated in Figure 3. The investigation on the formation of Schottky barriers in metal-semiconductor contacts has been widely studied for several decades because of its importance in the application of semiconductor devices [95]. Most work has focused on interfaces between metal electrodes and non-oxide semiconductors, e.g., Si and GaAs. In recent years, for oxide-based semiconductors, both of un-doped and doped-ZnO have greatly received significant interest. Based on Schottky–Mott theory, the Schottky barrier height for ideal contacts depends on the difference between the work function of the electron affinity of the semiconductor and the metal electrode only. It is commonly observed that the Schottky barrier height shows strong dependence not only on the type of metal electrodes but also on sample treatment. In the case of ZnO, the Schottky barrier height is greatly dependent on the conditions of sample treatment, such as ozone cleaning, plasma treatment, electrode deposition temperature, and subsequent thermal annealing [9,95,100].

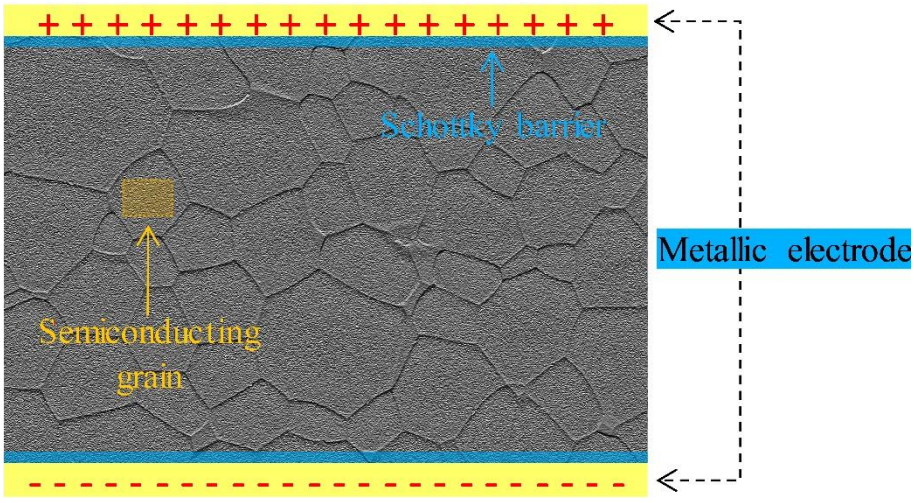

Figure 3 S-E effect consisting of semiconducting core and metallic electrode.

The weak sensitivity of the Schottky barrier height to the work function of the metal electrode, known as "Fermi-level pinning", and the strong dependence of SBH on sample treatment indicates that "interface states" such as interfacial bonding, surface defects, oxygen adsorption, and contamination also play an important role on the formation of Schottky barriers in such metal-semiconductor contacts. These complex and influential factors often make it challenging to produce stable and reproducible Ohmic/non-Ohmic contacts to leaky dielectrics/semiconducting oxides. Although the formation of Schottky barrier height can cause an extreme increase in the measured capacitance value (hence, dielectric permittivity), this is generally accompanied by a very high tanδ value.

1.4.2 Quasi-intrinsic: Electron-pinned defect-dipoles (EPDDs) effect

Hu et al. (2013) [3] reported an excellent novel material with dielectric properties in (In+Nb) co-doped rutile-TiO_2 ceramics. The $(In_{0.05}Nb_{0.05})_xTi_{1-x}O_2$ ceramic with x = 0.1 or refers to 10% (Nb+In) exhibited high ε' of ~6×10^4 with tanδ < 0.02 (at room temperature) over a frequency range of $10^2 – 10^6$ Hz. The In^{3+}-only doped rutile-TiO_2 ceramic exhibited a low ε' of about 120 at 1 kHz. Concurrently, Nb^{5+}-only doped rutile-TiO_2 ceramic exhibited a large ε' value, on the order of 10^4 over a wide frequency range ($10^2 – 10^6$ Hz). However, its tanδ value was found to be higher than 0.1. This large ε' value of the Nb^{5+}-only doped rutile-TiO_2 ceramic was ascribed to the effect of delocalized electron hopping, which usually accompanies high tanδ values. This indicates that In^{3+} doping ions play an important role in inhibiting transport due to localized electron hopping. Furthermore, it was also reported temperature independence of ε' over a wide temperature range from 80 to 450 K (or from -193 to 177 °C). In the temperature range of 450 – 720 K, ε' greatly increased. This was ascribed to DC conduction in the bulk ceramic and/or the dielectric relaxation process due to the ionic motion of oxygen vacancies. It is also interesting that giant-dielectric behavior can occur at a very low temperature (80 K at 100 kHz). This is rarely observed in other giant dielectric ceramics. For example, ε' at 100 kHz of a $CaCu_3Ti_4O_{12}$ ceramic starts to decrease at 150 – 200 K [1] rapidly.

These excellent dielectric properties are thought to originate from large defect-dipole clusters containing highly localized electrons. Doping dielectric rutile-TiO_2 ceramic with electron-donors such as Nb^{5+} can create conduction electrons by reducing Ti^{4+} to Ti^{3+}. While doping electron-acceptors such as In^{3+} into rutile-TiO_2 ceramic has little to no effect on the value of ε', it results in lower dielectric losses (tanδ) at higher frequencies. Examining the nominal composition of $(In_{0.05}Nb_{0.05})_xTi_{1-x}O_2$, the complex stoichiometry of $(In_x^{3+}Nb_x^{5+}Ti_x^{3+})Ti_{1-3x}^{4+}O_{2-x/2}$ produces defect clusters. The electrons created by both Nb^{5+} doping and the reduction of Ti^{4+} to Ti^{3+} in the close proximity to In^{3+}, as shown in Figure 4. Without the latter, electrons would delocalize and produce high tanδ values and strong-dependent high-ε'. This is a new model proposed as the origin of the giant dielectric response in ceramic oxides. An excellent-dielectric performance can be created by engineering a local structure within the structure of rutile-TiO_2.

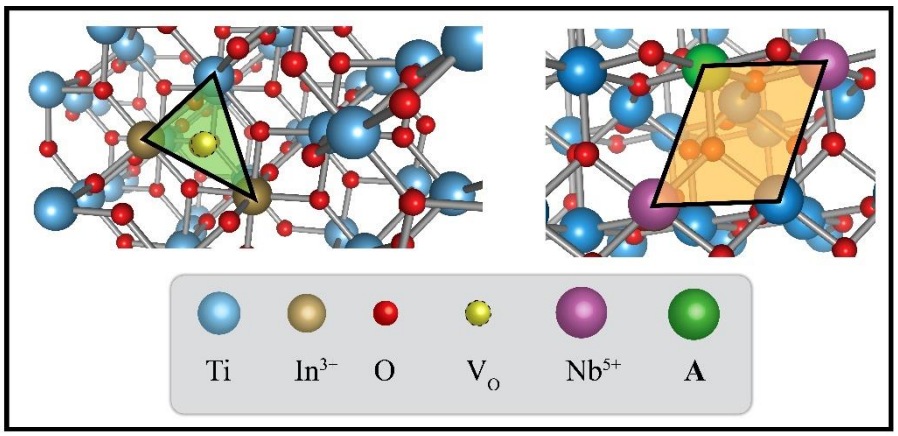

Figure 4 EPDD structure consisting of triangular $In_2^{3+}V_O^{\bullet\bullet}Ti^{3+}$ and diamond $Nb_2^{5+}Ti^{3+}A_{Ti}$.

2. Experimental

In this work, $Ti_{0.9875}Ta_{0.0125}O_{12}$, and $Ti_{1-x}(Ta_{0.5}In_{0.5})_xO_{12}$ (x = 0.01, 0.015, 0.025, and 0.05), as well as (In+Nb) and (Ga+Ta) co-doped TiO_2 ceramics, were successfully fabricated using a solid-state reaction (SSR) method. The starting raw metallic materials consist of TiO_2 (99.9% purity, Sigma-Aldrich), Ta_2O_5 (99.99% purity, Sigma-Aldrich), and In_2O_3 (99.99% purity, Sigma-Aldrich). To begin, the stoichiometric amount of starting raw metallic materials for each ceramic condition was mixed with C_2H_5OH (99.5% purity, RCI Labscan) in ball-milling bottles for 24 h at 150 rpm of a ball-milling rate. After that, the mixed raw materials were dried for 24 h at 80 °C in a heating oven. The dried powders were then crushed until smooth powders for each condition were obtained. Finally, the smooth powders were sieved to obtain the high-quality oxide powders. All powders were compressed into disks with a diameter of ~9.5 mm and a thickness of ~1.5 mm using uniaxial compression at 200 MPa. All green bodies were sintered in the air at various sintering temperatures and times, between 1200 and 1550 °C for 1 to 10 h.

All ceramics were analyzed for phase composition and crystalline structure using an X-ray diffractometer (XRD, EMPYREAN, PANalytical B.V.). The Rietveld refinement technique was used to examine the XRD spectra using the X'Pert HighScore Plus software version 3.0e. The microstructures and elemental distributions of the samples were analyzed using Field Emission Scanning Electron Microscopy (FE-SEM, FEI, Model: Helios NanoLab G3 CX) in conjunction with Energy-dispersive X-ray spectroscopy (EDS). X-ray photoemission spectroscopy (XPS, PHI5000 VersaProbe II, ULVAC-PHI) installed at Beamline 5.3 XPS, Synchrotron Light Research Institute (Public Organization), Nakhon Ratchasima, Thailand was used to determine the charge states of Ti and O ions. The MultiPak program based on Gaussian-Lorentzian profile fitting was used to analyze the XPS data.

Dielectric and electrical parameters were tested at various temperatures and frequencies using a KEYSIGHT E4990A at 0.5 V of oscillation voltage (V_{rms}). The metal electrodes on the sample surfaces were then coated. After that, all of the samples were burned in the air for 30 min at 600 °C. Dielectric measurement was measured in the frequency and temperature ranges of 40 – 10^7 Hz and -70 – 220 °C, respectively

3. Co-doped rutile-TiO_2

Initially, studies were conducted to determine the effect of various dopant types on the dielectric properties of TiO_2 based oxides. Figure 5 illustrates the dielectric properties of various types of co-doped TiO_2 ceramics at 25 °C.

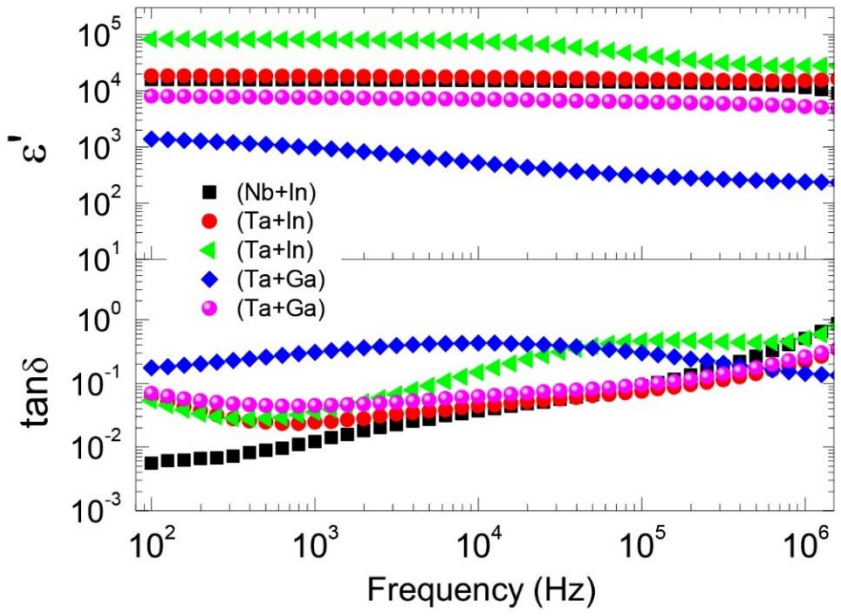

Figure 5 Dielectric properties (ε′ and tanδ) at 25 °C of various types of co-doped TiO_2 ceramics.

The upper frame illustrates the ε' function, while the lower frame illustrates the tanδ function as a function of frequency. As illustrated in this Figure 5, the dielectric response of co-doped TiO_2 is dependent on the metallic ion types added to the TiO_2 systems. The dielectric response of (Nb+In) co-doped TiO_2, denoted by the dark symbol, exhibits a high ε' of approximately 1.5×10^4 and a low tanδ about 0.01 at 1 kHz. In the case of (Ta+Ga) co-doped TiO_2, the ε' (~1.0 – 7.5×10^3) decreases while the tanδ (~0.045 – 0.30) increases in comparison to the previous case. Interestingly, when (Ta+In) co-doped TiO_2 is compared to (Nb+In) co-doped TiO_2, ε' increases significantly, while tanδ slightly increases. The ε' and tanδ values observed in (Ta+In) co-doped TiO_2 were $2.0 – 8.0 \times 10^4$ and 0.025 – 0.035, respectively. As revealed in the result, each co-doping ceramic condition can exhibit exceptional dielectric behavior on its own. Interestingly, the dielectric properties of (Ta+In) co-doped TiO_2, particularly the tanδ value, could be suitable for practical capacitor applications [26]. As a result, we chose to investigate the (Ta+In) co-doped TiO_2 further in this work, with a particular emphasis on the effects of different doping concentrations and sintering conditions on the dielectric performance at room temperature and over a wide temperature range.

In the crystalline structure study, we discovered that all ceramics show a single phase of rutile-TiO_2 with JCPDS No. 21–1276 in the (Ta+In) co-doped TiO_2 study. All ceramics were free of any possible impurities. This discovery points to perfect Ta^{5+} and In^{3+} substitutions in Ti^{4+} sites. The lattice parameters (a) of co-doped TiO_2 ceramics with various doping concentrations were calculated and compared to the standard structure, revealing that they have larger the a values than pure rutile-TiO_2 ceramics. The larger ionic radii of In^{3+} (r_{In} = 0.80 Å) and Ta^{5+} (r_{Ta} = 0.78 Å) than that of the host Ti^{4+} ion (r_{Ti} = 0.605 Å) could contribute for the increase of the a values [101]. The EDS mapping method was utilized to examine the dispersions of base and doping elements. As seen in Figure 6, the dispersions of Ti, Ta, In, and O are relatively homogenous. This EDS mapping shows that small concentrations of Ta^{5+} and In^{3+} doping ions can fill Ti^{4+} host sites.

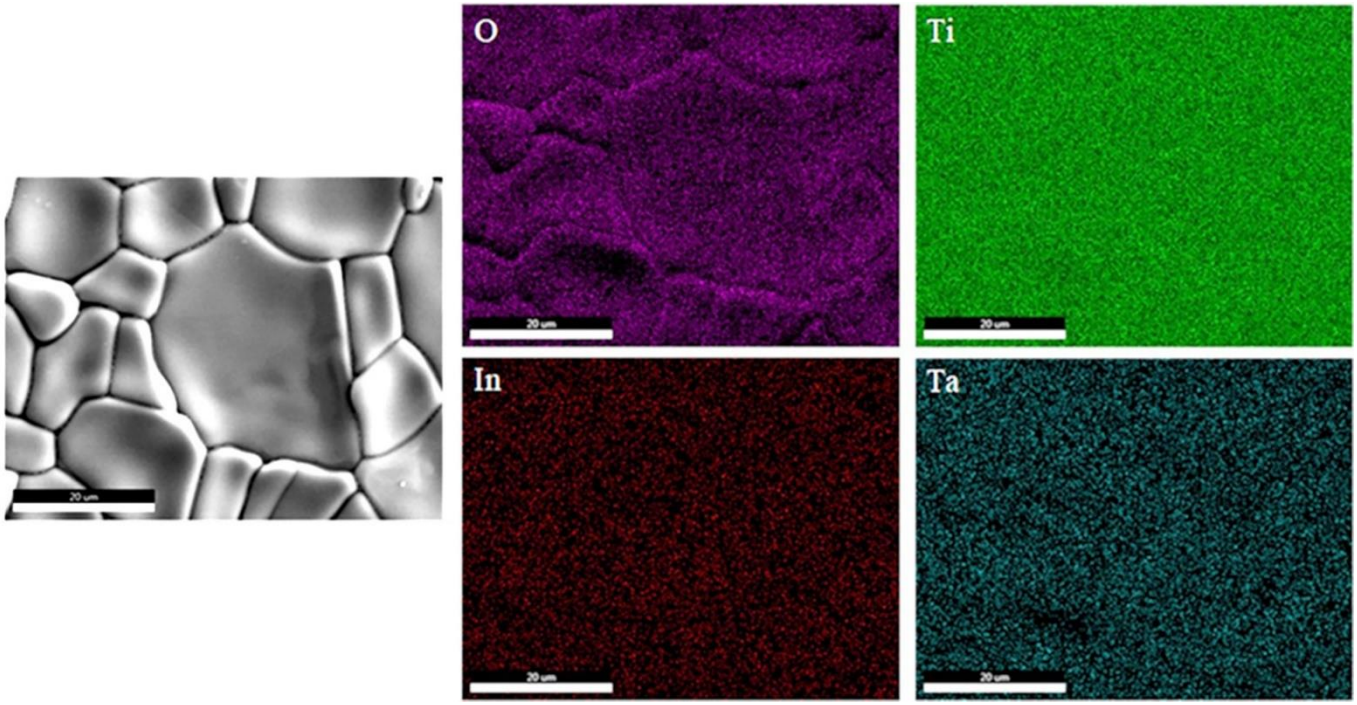

Figure 6 SEM mapping images of In+Ta co-doped TiO_2 ceramics.

Figure 7 shows the frequency dependences of the dielectric parameters ε' and tanδ of Ta^{5+} single doped TiO_2 and (Ta+In) co-doped TiO_2 sintered at 1550 °C for 1 h at 25 °C. As shown in this graph, single doping, 1.25% Ta sample can have the highest ε' while also having the highest low-frequency tanδ. Due to charge balance, it is reasonable to believe that doping with Ta^{5+} can cause Ti^{4+} to change to Ti^{3+}. As a result, the small conductivity in this sample due to short-range charge migration may increase when compared to others [102]. Increases in ε' and tanδ could be aided in this manner. This ceramic exhibits two relaxations, the first of which occurs at ~10^4 Hz and the second of which occurs at ~5×10^5 Hz. Also, two relaxations were observed in the 5.0% (Ta+In) ceramic.

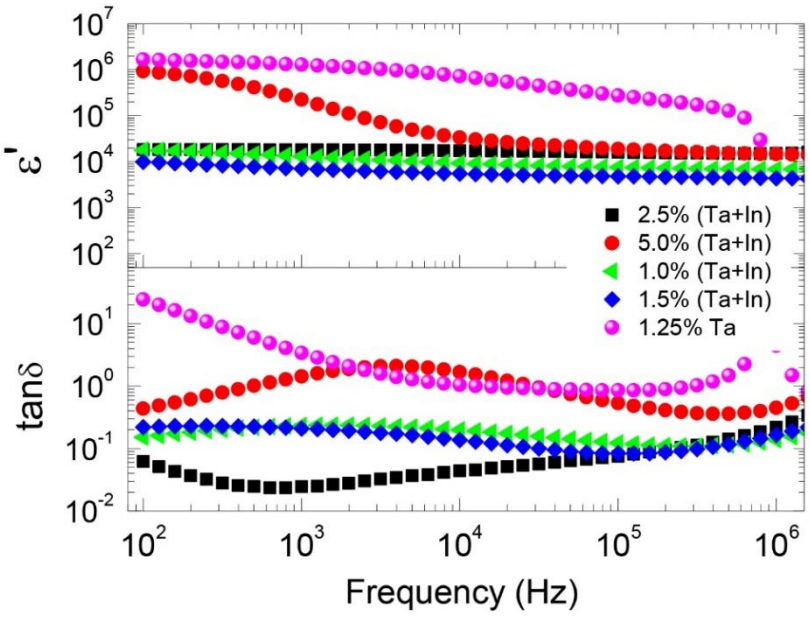

Figure 7 Dielectric properties (ε' and tanδ) at 25 °C of In+Ta co-doped TiO_2 ceramics with different co-doping concentrations compared to that of Ta-doped TiO_2.

As shown in this Figure 7, the ε' and tanδ in a frequency range below 10^3 Hz are lower in the co-doped TiO_2 ceramics than they are in the 1.25% Ta sample, which is interesting. This behavior is similar to that of (Nb+In) co-doped TiO_2 reported in the literature [3]. We adjusted the doping concentration to improve the dielectric and electrical properties of TiO_2 base oxides in this research. The finding reveals that the dielectric properties of (Ta+In) co-doped TiO_2 vary with doping concentration. In the 2.5% (Ta+In) ceramic, good dielectric properties with high ε' ~1.81×10^4 and low tanδ ~0.025 were achieved. The low tanδ while maintaining a high ε' value in this ceramic may be due to the appropriate doping concentration causing high insulative states while maintaining a high dielectric polarization density in this ceramic.

The 2.5% (Ta+In) powder was shaped into pellets and sintered under different sintering parameters in order to optimize the sintering condition in order to acquire the optimum dielectric properties. The result is shown in Figure 8. In the ceramics sintered for 5 h, grain sizes of 2.5% (Ta+In) ceramic increase significantly as increasing sintering temperature (1300 °C → 1400 °C → 1500 °C → 1550 °C). Also, the grain size of the 2.5% (Ta+In) ceramic sintered at 1550 °C for 1 h is bigger than that of the ceramic sintered at 1300 and 1400 °C for 5 h. Figure 8 shows the frequency dependences of ε' and tanδ at 30 °C of the 2.5% (Ta+In) ceramics sintered for 5 h at 1300, 1400, 1500, and 1550 °C, and for 1 h at 1550 °C. All ceramics have enormous dielectric properties, with ε' values in the order of 10^4. Over the observed frequency range, the ε' of the 2.5% (Ta+In) ceramics rose with increasing mean grain size, which was driven by sintering temperature. This is also comparable to the phenomena found in CCTO and related oxides, as described by the IBLC

dielectric model [62,64,68]. As shown in the tanδ spectra, the tanδ at 100 Hz increases significantly as the sintering temperature rises. At the standard frequency for use in capacitor applications, which is 1 kHz, the tanδ values of the 2.5% (Ta+In) ceramics sintered at 1400 °C for 5 h and 1550 °C for 1 h are very low compared to the others. The ε′ at 1 kHz and 30 °C of the 2.5% (Ta+In) ceramics sintered at 1400 °C for 5 h and 1550 °C for 1 h are 1.28×10^4 and 1.70×10^4, respectively. For the 2.5% (Ta+In) ceramics sintered at 1400 °C for 5 h and 1550 °C for 1 h, their measured tanδ values were 0.018 and 0.006, respectively. These values for ε′ and tanδ are commensurate with the industry standard for ceramic capacitor applications [26].

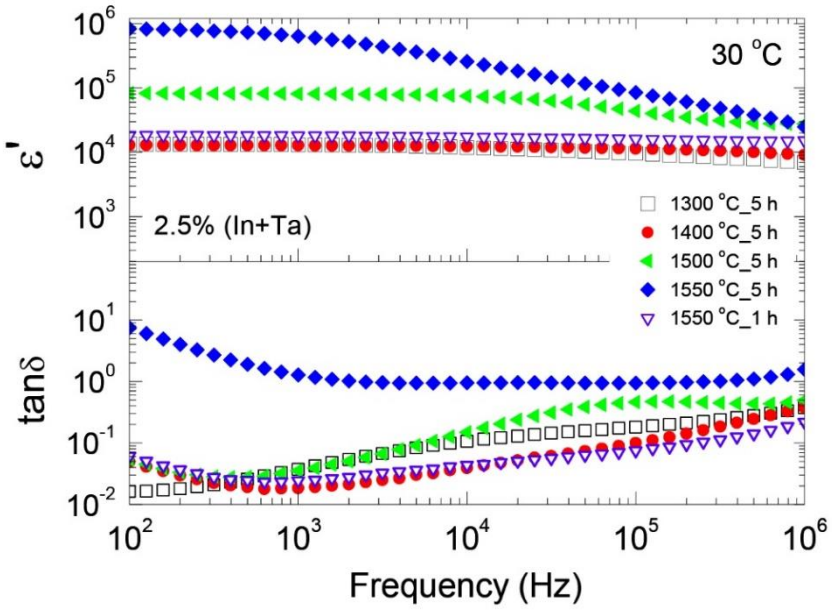

Figure 8 Dielectric properties (ε′ and tanδ) at 25 °C of In+Ta co-doped TiO_2 ceramics sintered under different conditions.

In Figure 9, the variation of ε′ value and the temperature coefficient of all samples were examined. At 1 kHz, it was discovered that the ε′ of 2.5% (Ta+In) ceramics sintered at 1400 °C for 5 h and 1550 °C for 1 h is strongly independent of temperature throughout the temperature range of -70 – 220 °C, whereas the ε′ of ceramics sintered at 1300 and 1500 °C for 5 h is slightly dependent as temperature changes, as shown in Figure 9(a). 2.5% (Ta+In) ceramic sintered at 1550 °C for 5 h showed the greatest dependence on the temperature of ε′. The temperature coefficient ε′ ($\Delta\varepsilon'/\varepsilon'_{20}$(%)) was calculated and plotted in Figure 9(b). It was discovered that ceramics sintered at 1400 °C for 5 h and 1500 °C for 1 h have excellent temperature coefficient properties. Additionally, we have found that the ceramic sintered at 1400 °C for 5 h and 1500 °C for 1 h had a temperature coefficient of less than 15% in the ranges of -70 – 200 °C and -70 – 190 °C, respectively. These two ceramics' superior thermal stability indicates their suitability for use in high-temperature electronic applications. This temperature stability meets at least X8R or higher capacitor application specifications [26]. These findings have not been seen in other materials, including CCTO and $BaTiO_3$ based oxides [62,64,68,103,104]. The nonlinear current density (J) – electric field (E) characteristics of a 2.5% (Ta+In) ceramic sintered at 1400 °C for 5 h [the inset of Figure 9(a)]. The relationship between J and E was discovered to be nonlinear. Additionally, we compared the J – E curves of 2.5% (Ta+In) ceramic to those of 2.5% (Nb+In) ceramic and discovered that the breakdown electric field (E_b) of 2.5% (Ta+In) ceramic is greater than that of 2.5% (Nb+In) ceramic, indicating a higher breakdown strength in the 2.5% (Ta+In) ceramic sample.

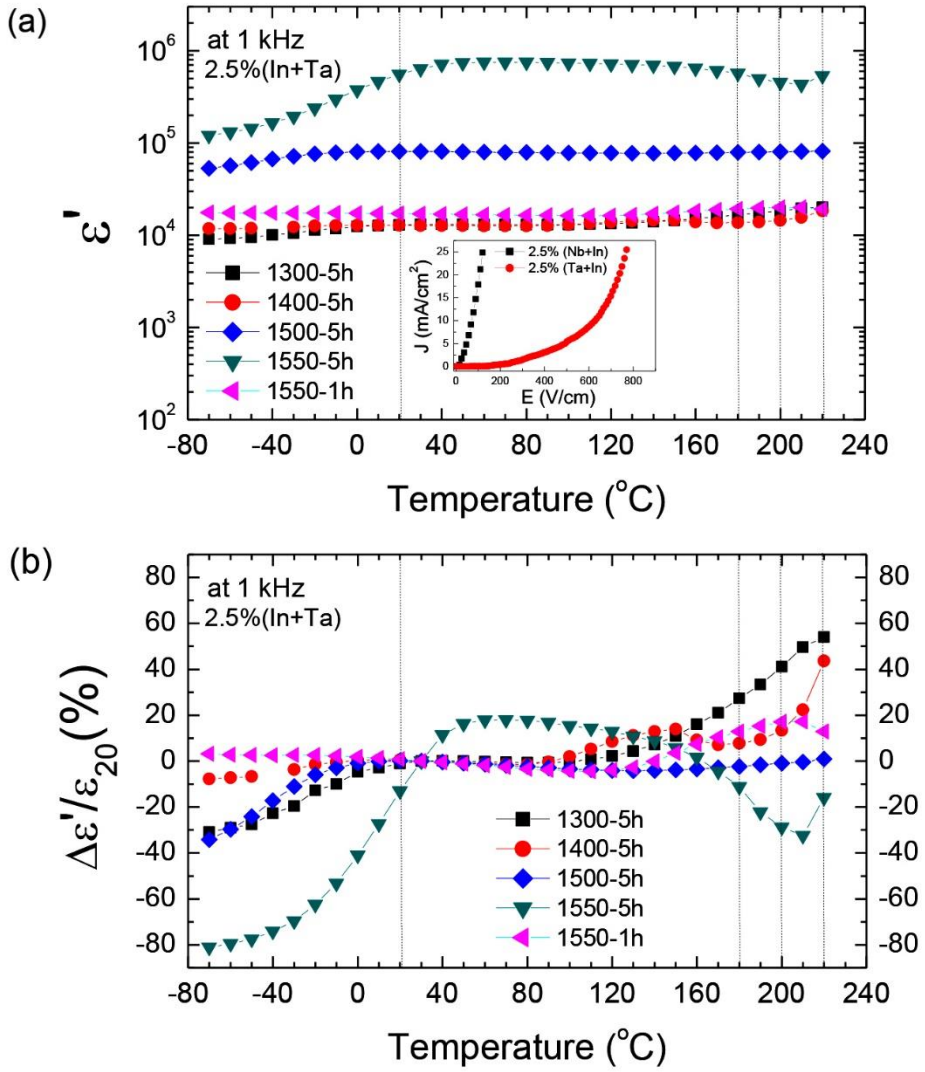

Figure 9 (a) Temperature dependence of ε′ at 1 kHz of In+Ta co-doped TiO_2 ceramics sintered under different conditions. (b) Temperature coefficient of ε′ at 1 kHz.

As seen in Figure 10, the XPS Ti2*p* spectrum of the (Ta+In) co-doped TiO_2 sample demonstrates the occurrence of Ti^{3+}/Ti^{4+} mixing. The primary peak corresponding to Ti^{4+} was discovered at binding energy (BE) of 458.7 eV, whereas the minor peak corresponding to Ti^{3+} was discovered at a BE of 457.3 eV. The valence state transition of Ti ions from Ti^{4+} to Ti^{3+} occurs at a ratio of around 100:1.2. The charge compensation processes associated with charge balancing are the major mechanism of valence state change.

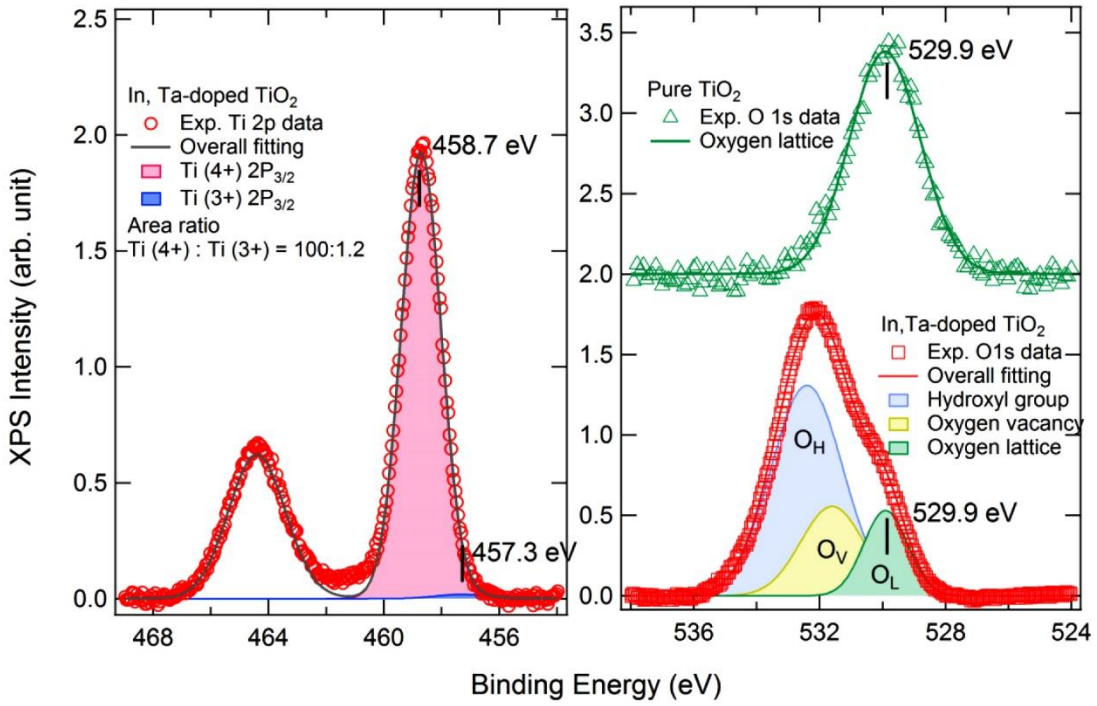

Figure 10 XPS spectra for Ti 2*p* and O 1*s* for In+Ta co-doped TiO_2 ceramics compared to that of pure TiO_2.

According to the replacement of Ta^{5+} into the Ti^{4+} sites of the rutile-TiO_2, free electrons can be generated by reducing Ti^{4+} to Ti^{3+}, as follows.

$$Ta_2O_5 + 2TiO_2 \xrightarrow{4TiO_2} 2Ta_{Ti}^{\bullet} + 2Ti_{Ti}' + 8O_o + \frac{1}{2}O_2 \quad (2)$$

$$Ti^{4+} + e \longrightarrow Ti^{3+} \quad (3)$$

Equations (2) and (3) demonstrate that doping with Ta^{5+} can induce free electrons in (Ta+In) co-doped TiO_2. As demonstrated in the XPS O 1*s* spectra, the undoped TiO_2 exhibits the main oxygen lattice (O_L) peak at BE position of 529.9 eV. In contrast, the XPS O 1*s* spectrum of (Ta+In) co-doped TiO_2 sample is in an asymmetric shape. As shown by the fitting line, it is composed of 3 components: the O_L, oxygen vavancy (O_V), and a surface hydroxyl (O_H). The O_V cannot be induced by doping Ta^{5+} in general. Thus, the replacement of In^{3+} into the Ti^{4+} sites of TiO_2 may increase the number of O_V as compared to a pure TiO_2 system, as indicated by the following relationship.

$$In_2O_3 + 2TiO_2 \longrightarrow 2In_{Ti}' + V_O^{\bullet\bullet} + 3O_O \quad (4)$$

As shown by the XPS spectra, the EPDD model may be the primary origin of the high ε' and low tanδ in (Ta+In) co-doped TiO_2. When triangular-shaped $In_2^{3+}V_O^{\bullet\bullet}Ti^{3+}$ and diamond-shaped $Ta_2^{5+}Ti^{3+}A_{Ti}$ (A = Ti^{3+}, In^{3+}, or Ti^{4+})

intrinsic defect complexes are substantially coupled or overlapped [3], high ε' and low tanδ can be formed. However, as reported in our previous work, (Nb+In) co-doped CCTO [21], the SBLC model was proposed to be a significant influence in the apparent low tanδ values in co-doped TiO_2 ceramics. As a result, the perspective may be examined further in the subsequent study.

4. Conclusion

The GDPs of many oxides that have been reported in recent years were associated with the formation of Schottky barriers at internal interfaces. Hence, the interfacial polarization at internal interfaces gave rise to the observed GDP behavior. The EPDDs, which may be induced in some dielectric oxides, were also proposed to the observed GDP with very low tanδ. Although the origins of the GDP with the excellent dielectric performance of many co-doped TiO_2 systems are still unclear now, the obtained excellent dielectric performance is valuable for further development in ceramic capacitors.

.

Acknowledgment

This project is funded by the National Research Council of Thailand (NRCT): (N41A640084). Funding support has also been received from the National Science, Research and Innovation Fund (NSRF) and the Basic Research Fund of Khon Kaen University.

References

[1] C. C. Homes, T. Vogt, S. M. Shapiro, S. Wakimoto, A. P. Ramirez, Optical response of high-dielectric-constant perovskite-related oxide, *Science* **293** (2001) 673-676.

[2] J. Wu, C.-W. Nan, Y. Lin, Y. Deng, Giant dielectric permittivity observed in Li and Ti doped NiO, *Phys. Rev. Lett.* **89** (2002) 217601.

[3] W. Hu, Y. Liu, R. L. Withers, T. J. Frankcombe, L. Norén, A. Snashall, M. Kitchin, P. Smith, B. Gong, H. Chen, J. Schiemer, F. Brink, J. Wong-Leung, Electron-pinned defect-dipoles for high-performance colossal permittivity materials, *Nat. Mater.* **12** (2013) 821-826.

[4] S. Krohns, P. Lunkenheimer, S. Meissner, A. Reller, B. Gleich, A. Rathgeber, T. Gaugler, H. U. Buhl, D. C. Sinclair, A. Loidl, The route to resource-efficient novel materials, *Nat. Mater.* **10** (2011) 899-901.

[5] C. C. Homes, T. Vogt, Colossal permittivity materials: Doping for superior dielectrics, *Nat. Mater.* **12** (2013) 782-783.

[6] Y. Wang, W. Jie, C. Yang, X. Wei, J. Hao, Colossal permittivity materials as superior dielectrics for diverse applications, *Adv. Funct. Mater.* **29** (2019) 1808118.

[7] M. A. Subramanian, D. Li, N. Duan, B. A. Reisner, A. W. Sleight, High dielectric constant in $ACu_3Ti_4O_{12}$ and $ACu_3Ti_3FeO_{12}$ phases, *J. Solid State Chem.* **151** (2000) 323-325.

[8] D. C. Sinclair, T. B. Adams, F. D. Morrison, A. R. West, $CaCu_3Ti_4O_{12}$: One-step internal barrier layer capacitor, *Appl. Phys. Lett.* **80** (2002) 2153.

[9] P. Lunkenheimer, R. Fichtl, S. Ebbinghaus, A. Loidl, Nonintrinsic origin of the colossal dielectric constants in $CaCu_3Ti_4O_{12}$, *Phys. Rev. B* **70** (2004) 172102.

[10] S. Sarkar, P. K. Jana, B. K. Chaudhuri, H. Sakata, Copper (II) oxide as a giant dielectric material, *Appl. Phys. Lett.* **89** (2006) 212905.

[11] S. Krohns, P. Lunkenheimer, C. Kant, A. V. Pronin, H. B. Brom, A. A. Nugroho, M. Diantoro, A. Loidl, Colossal dielectric constant up to gigahertz at room temperature, *Appl. Phys. Lett.* **94** (2009) 122903.

[12] T. Park, Z. Nussinov, K. Hazzard, V. Sidorov, A. Balatsky, J. Sarrao, S. W. Cheong, M. Hundley, J.-S. Lee, Q. Jia, J. Thompson, Novel dielectric anomaly in the hole-doped $La_2Cu_{1-x}Li_xO_4$ and $La_{2-x}Sr_xNiO_4$ insulators: Signature of an electronic glassy state, *Phys. Rev. Lett.* **94** (2005) 017002.

[13] M. C. Ferrarelli, T. B. Adams, A. Feteira, D. C. Sinclair, A. R. West, High intrinsic permittivity in $Na_{1/2}Bi_{1/2}Cu_3Ti_4O_{12}$, *Appl. Phys. Lett.* **89** (2006) 212904.

[14] I. P. Raevski, S. A. Prosandeev, A. S. Bogatin, M. A. Malitskaya, L. Jastrabik, High dielectric permittivity in $AFe_{1/2}B_{1/2}O_3$ nonferroelectric perovskite ceramics (A = Ba, Sr, Ca; B = Nb, Ta, Sb), *J. Appl. Phys.* **93** (2003) 4130-4136.

[15] W. Dong, W. Hu, A. Berlie, K. Lau, H. Chen, R. L. Withers, Y. Liu, Colossal dielectric behavior of Ga+Nb Co-doped rutile TiO_2, *ACS Appl. Mater. Interfaces* **7** (2015) 25321-25325.

[16] C. Zhao, J. Wu, Effects of secondary phases on the high-performance colossal permittivity in titanium dioxide ceramics, *ACS Appl. Mater. Interfaces* **10** (2018) 3680-3688.

[17] Z. Li, J. Wu, D. Xiao, J. Zhu, W. Wu, Colossal permittivity in titanium dioxide ceramics modified by tantalum and trivalent elements, *Acta Mater.* **103** (2016) 243-251.

[18] X. Cheng, Z. Li, J. Wu, Colossal permittivity in ceramics of TiO_2 co-doped with niobium and trivalent cation, *J. Mater. Chem. A* **3** (2015) 5805-5810.

[19] W. Dong, W. Hu, T. J. Frankcombe, D. Chen, C. Zhou, Z. Fu, L. Candido, G. Hai, H. Chen, Y. Li, R. L. Withers, Y. Liu, Colossal permittivity with ultralow dielectric loss in In+Ta co-doped rutile TiO_2, *J. Mater. Chem. A* **5** (2017) 5436-5441.

[20] C. Yang, M.-Y. Tse, X. Wei, J. Hao, Colossal permittivity of (Mg+Nb) co-doped TiO_2 ceramics with low dielectric loss, *J. Mater. Chem. C* **5** (2017) 5170-5175.

[21] T. Nachaithong, P. Kidkhunthod, P. Thongbai, S. Maensiri, Surface barrier layer effect in (In+Nb) co-doped TiO_2 ceramics: An alternative route to design low dielectric loss, *J. Am. Ceram. Soc.* **100** (2017) 1452-1459.

[22] W. Tuichai, S. Danwittayakul, N. Chanlek, P. Srepusharawoot, P. Thongbai, S. Maensiri, Origin(s) of the apparent colossal permittivity in $(In_{1/2}Nb_{1/2})_xTi_{1-x}O_2$: Clarification on the strongly induced Maxwell-Wagner polarization relaxation by DC bias, *RSC Adv.* **7** (2017) 95-105.

[23] W. Dong, D. Chen, W. Hu, T. J. Frankcombe, H. Chen, C. Zhou, Z. Fu, X. Wei, Z. Xu, Z. Liu, Y. Li, Y. Liu, Colossal permittivity behavior and its origin in rutile $(Mg_{1/3}Ta_{2/3})_xTi_{1-x}O_2$, *Sci. Rep.* **7** (2017) 9950.

[24] X. Wang, B. Zhang, L. Xu, X. Wang, Y. Hu, G. Shen, L. Sun, Dielectric properties of Y and Nb co-doped TiO_2 ceramics, *Sci. Rep.* **7** (2017) 8517.

[25] W. Hu, L. Li, G. Li, Y. Liu, R. L. Withers, Atomic-scale control of TiO(6) octahedra through solution chemistry towards giant dielectric response, *Sci Rep.* **4** (2014) 6582.

[26] A. J. Moulson, J. M. Herbert, Electroceramics: Materials, properties, applications, 2nd ed., West Sussex, UK: Wiley (2003).

[27] S.-Y. Chung, I.-D. Kim, S.-J. L. Kang, Strong nonlinear current–voltage behaviour in perovskite-derivative calcium copper titanate, *Nat. Mater.* **3** (2004) 774-778.

[28] W. Somphan, N. Sangwong, T. Yamwong, P. Thongbai, Giant dielectric and electrical properties of sodium yttrium copper titanate: $Na_{1/2}Y_{1/2}Cu_3Ti_4O_{12}$, *J. Mater. Sci.: Mater. Electron.* **23** (2012) 1229-1234.

[29] W. Somphan, P. Thongbai, T. Yamwong, S. Maensiri, High Schottky barrier at grain boundaries observed in $Na_{1/2}Sm_{1/2}Cu_3Ti_4O_{12}$ ceramics, *Mater. Res. Bull.* **48** (2013) 4087-4092.

[30] P. Thongbai, T. Yamwong, S. Maensiri, Dielectric properties and electrical response of grain boundary of $Na_{1/2}La_{1/2}Cu_3Ti_4O_{12}$ ceramics, *Mater. Res. Bull.* **47** (2012) 432-437.

[31] R. Schmidt, M. C. Stennett, N. C. Hyatt, J. Pokorny, J. Prado-Gonjal, M. Li, D. C. Sinclair, Effects of sintering temperature on the internal barrier layer capacitor (IBLC) structure in $CaCu_3Ti_4O_{12}$ (CCTO) ceramics, *J. Eur. Ceram. Soc.* **32** (2012) 3313-3323.

[32] J. Jumpatam, N. Chanlek, M. Takesada, P. Thongbai, Giant dielectric behavior of monovalent cation/anion (Li^+, F^-) co-doped $CaCu_3Ti_4O_{12}$ ceramics, *J. Am. Ceram. Soc.* **103** (2020) 1871-1880.

[33] Z. Peng, D. Wu, P. Liang, X. Zhou, J. Wang, J. Zhu, X. Chao, Z. Yang, Grain boundary engineering that induces ultrahigh permittivity and decreased dielectric loss in $CdCu_3Ti_4O_{12}$ ceramics, *J. Am. Ceram. Soc.* **103** (2020) 1230-1240.

[34] E. C. Grzebielucka, J. F. H. L. Monteiro, E. C. F. de Souza, C. P. F. Borges, A. V. C. de Andrade, E. Cordoncillo, H. Beltrán-Mir, S. R. M. Antunes, Improvement in varistor properties of $CaCu_3Ti_4O_{12}$ ceramics by chromium addition, *J. Mater. Sci. Technol.* **41** (2020) 12-20.

[35] J. Jumpatam, N. Chanlek, P. Thongbai, Giant dielectric response, electrical properties and nonlinear current-voltage characteristic of Al_2O_3-$CaCu_3Ti_4O_{12}$ nanocomposites, *Appl. Surf. Sci.* **476** (2019) 623-631.

[36] L. Liu, S. Ren, J. Liu, F. Han, J. Zhang, B. Peng, D. Wang, A. A. Bokov, Z. G. Ye, Localized polarons and conductive charge carriers: Understanding $CaCu_3Ti_4O_{12}$ over a broad temperature range, *Phys. Rev. B* **99** (2019) 094110.

[37] J. Wang, Z. Lu, Z. Chen, The novel effects of Cu-deficient on the dielectric properties and voltage–current nonlinearity in $CaCu_3Ti_4O_{12}$ ceramics, *Mater. Sci. Eng. B* **243** (2019) 1-7.

[38] X. Wang, P. Liang, Z. Peng, H. Peng, Y. Xiang, X. Chao, Z. Yang, Significantly enhanced breakdown electric field in Zn-doped $Y_{2/3}Cu_3Ti_4O_{12}$ ceramics, *J. Alloys Compd.* **778** (2019) 391-397.

[39] N. Zhao, P. Liang, D. Wu, X. Chao, Z. Yang, Temperature stability and low dielectric loss of lithium-doped $CdCu_3Ti_4O_{12}$ ceramics for X9R capacitor applications, *Ceram. Int.* **45** (2019) 22991-22997.

[40] A. Cho, C. S. Han, M. Kang, W. Choi, J. Lee, J. Jeon, S. Yu, Y. S. Jung, Y. S. Cho, Direct correlations of grain boundary potentials to chemical states and dielectric properties of doped $CaCu_3Ti_4O_{12}$ thin films, *ACS Appl. Mater. Interfaces* **10** (2018) 16203-16209.

[41] Z. Tang, Y. Huang, K. Wu, J. Li, Significantly enhanced breakdown field in $Ca_{1-x}Sr_xCu_3Ti_4O_{12}$ ceramics by tailoring donor densities, *J. Eur. Ceram. Soc.* **38** (2018) 1569-1575.

[42] P. Thongbai, S. Maensiri, T. Yamwong, Effects of grain, grain boundary, and dc electric field on giant dielectric response in high purity CuO ceramics, *J. Appl. Phys.* **104** (2008) 036107.

[43] P. Thongbai, T. Yamwong, S. Maensiri, Correlation between giant dielectric response and electrical conductivity of CuO ceramic, *Solid State Commun.* **147** (2008) 385-387.

[44] P. Thongbai, T. Yamwong, S. Maensiri, Microstructure and modified giant dielectric response in Ga-doped $La_{1.5}Sr_{0.5}NiO_4$ ceramics, *Mater. Lett.* **82** (2012) 244-247.

[45] K. Meeporn, T. Yamwong, P. Thongbai, $La_{1.7}Sr_{0.3}NiO_4$ nanocrystalline powders prepared by a combustion method using urea as fuel: Preparation, characterization, and their bulk colossal dielectric constants, *Jpn. J. Appl. Phys.* **53** (2014) 06JF01.

[46] X. Q. Liu, B. W. Jia, W. Z. Yang, J. P. Cheng, X. M. Chen, Dielectric relaxation and polaronic hopping in Al-substituted $Sm_{1.5}Sr_{0.5}NiO_4$ ceramics, *J. Phys. D: Appl. Phys.* **43** (2010) 495402.

[47] B. W. Jia, W. Z. Yang, X. Q. Liu, X. M. Chen, Giant dielectric response in $(Sm_{1-x}Nd_x)_{1.5}Sr_{0.5}NiO_4$ ceramics: The intrinsic and extrinsic effects, *J. Appl. Phys.* **112** (2012) 024104.

[48] X. Q. Liu, S. Y. Wu, X. M. Chen, Enhanced giant dielectric response in Al-substituted $La_{1.75}Sr_{0.25}NiO_4$ ceramics, *J. Alloys Compd.* **507** (2010) 230-235.

[49] K. Meeporn, N. Chanlek, P. Thongbai, Effects of DC bias on non-ohmic sample-electrode contact and grain boundary responses in giant-permittivity $La_{1.7}Sr_{0.3}Ni_{1-x}Mg_xO_4$ ceramics, *RSC Adv.* **6** (2016) 91377-91385.

[50] T. I. Chupakhina, N. I. Kadyrova, N. V. Melnikova, O. I. Gyrdasova, E. A. Yakovleva, Y. G. Zainulin, New methods for the preparation and dielectric properties of $La_{2-x}Sr_xNiO_4$ (x = 1/8) ceramic, *Mater. Res. Bull.* **77** (2016) 190-198.

[51] Y. Lin, J. Wang, L. Jiang, Y. Chen, C.-W. Nan, High permittivity Li and Al doped NiO ceramics, *Appl. Phys. Lett.* **85** (2004) 5664.

[52] Y.-J. Hsiao, Y.-S. Chang, T.-H. Fang, Y.-L. Chai, C.-Y. Chung, Y.-H. Chang, High dielectric permittivity of Li and Ta codoped NiO ceramics, *J. Phys. D: Appl. Phys.* **40** (2007) 863-868.

[53] P. K. Jana, S. Sarkar, B. K. Chaudhuri, H. Sakata, Effect of dc electric field on conductivity and giant permittivity of $K_xTi_yNi_{1-x-y}O$, *Appl. Phys. Lett.* **90** (2007) 242913.

[54] P. K. Jana, S. Sarkar, H. Sakata, T. Watanabe, B. K. Chaudhuri, Microstructure and dielectric properties of $Na_xTi_yNi_{1-x-y}O$ (x = 0.05–0.30, y = 0.02), *J. Phys. D: Appl. Phys.* **41** (2008) 065403.

[55] P. Thongbai, S. Pongha, T. Yamwong, S. Maensiri, Effects of Fe, Ti, and V doping on the microstructure and electrical properties of grain and grain boundary of giant dielectric NiO-based ceramics, *Appl. Phys. Lett.* **94** (2009) 022908.

[56] S. Pongha, P. Thongbai, T. Yamwong, S. Maensiri, Giant dielectric response and polarization relaxation mechanism in (Li,V)-doped NiO ceramics, *Scr. Mater.* **60** (2009) 870-873.

[57] Z. Wang, X. M. Chen, L. Ni, Y. Y. Liu, X. Q. Liu, Dielectric relaxations in $Ba(Fe_{1/2}Ta_{1/2})O_3$ giant dielectric constant ceramics, *Appl. Phys. Lett.* **90** (2007) 102905.

[58] Y. Y. Liu, X. M. Chen, X. Q. Liu, L. Li, Dielectric relaxations in $Ca(Fe_{1/2}Nb_{1/2})O_3$ complex perovskite ceramics, *Appl. Phys. Lett.* **90** (2007) 262904.

[59] Y. Y. Liu, X. M. Chen, X. Q. Liu, L. Li, Giant dielectric response and relaxor behaviors induced by charge and defect ordering in $Sr(Fe_{1/2}Nb_{1/2})O_3$ ceramics, *Appl. Phys. Lett.* **90** (2007) 192905.

[60] N. Ikeda, H. Ohsumi, K. Ohwada, K. Ishii, T. Inami, K. Kakurai, Y. Murakami, K. Yoshii, S. Mori, Y. Horibe, H. Kito, Ferroelectricity from iron valence ordering in the charge-frustrated system $LuFe_2O_4$, *Nature* **436** (2005) 1136-1138.

[61] C. Pecharromán, F. Esteban-Betegón, J. F. Bartolomé, S. López-Esteban, J. S. Moya, New percolative $BaTiO_3$–Ni composites with a high and frequency-independent dielectric constant ($\epsilon_r \approx 80000$), *Adv. Mater.* **13** (2001) 1541-1544.

[62] J. Boonlakhorn, P. Thongbai, B. Putasaeng, T. Yamwong, S. Maensiri, Very high-performance dielectric properties of $Ca_{1-3x/2}Yb_xCu_3Ti_4O_{12}$ ceramics, *J. Alloys Compd.* **612** (2014) 103-109.

[63] J. Jumpatam, B. Putasaeng, T. Yamwong, P. Thongbai, S. Maensiri, A novel route to greatly enhanced dielectric permittivity with reduce loss tangent in $CaCu_{3-x}Zn_xTi_4O_{12}/CaTiO_3$ composites, *J. Am. Ceram. Soc.* **97** (2014) 2368-2371.

[64] Z. Yang, L. Zhang, X. Chao, L. Xiong, J. Liu, High permittivity and low dielectric loss of the $Ca_{1-x}Sr_xCu_3Ti_4O_{12}$ ceramics, *J. Alloys Compd.* **509** (2011) 8716-8719.

[65] S. F. Shao, J. L. Zhang, P. Zheng, C. L. Wang, J. C. Li, M. L. Zhao, High permittivity and low dielectric loss in ceramics with the nominal compositions of $CaCu_{3-x}La_{2x/3}Ti_4O_{12}$, *Appl. Phys. Lett.* **91** (2007) 042905.

[66] W. Kobayashi, I. Terasaki, $CaCu_3Ti_4O_{12}/CaTiO_3$ composite dielectrics: Ba/Pb-free dielectric ceramics with high dielectric constants, *Appl. Phys. Lett.* **87** (2005) 032902.

[67] S. Vangchangyia, T. Yamwong, E. Swatsitang, P. Thongbai, S. Maensiri, Selectivity of doping ions to effectively improve dielectric and non-ohmic properties of $CaCu_3Ti_4O_{12}$ ceramics, *Ceram. Int.* **39** (2013) 8133-8139.

[68] Y. Li, P. Liang, X. Chao, Z. Yang, Preparation of $CaCu_3Ti_4O_{12}$ ceramics with low dielectric loss and giant dielectric constant by the sol–gel technique, *Ceram. Int.* **39** (2013) 7879-7889.

[69] S. Vangchangyia, E. Swatsitang, P. Thongbai, S. Pinitsoontorn, T. Yamwong, S. Maensiri, V. Amornkitbamrung, P. Chindaprasirt, Very low loss tangent and high dielectric permittivity in pure-$CaCu_3Ti_4O_{12}$ ceramics prepared by a modified sol-gel process, *J. Am. Ceram. Soc.* **95** (2012) 1497-1500.

[70] Z.-M. Dang, T. Zhou, S.-H. Yao, J.-K. Yuan, J.-W. Zha, H.-T. Song, J.-Y. Li, Q. Chen, W.-T. Yang, J. Bai, Advanced calcium copper titanate/polyimide functional hybrid films with high dielectric permittivity, *Adv. Mater.* **21** (2009) 2077-2082.

[71] M. Arbatti, X. Shan, Z. Y. Cheng, Ceramic–polymer composites with high dielectric constant, *Adv. Mater.* **19** (2007) 1369-1372.

[72] B.-H. Fan, J.-W. Zha, D. Wang, J. Zhao, Z.-M. Dang, Size-dependent low-frequency dielectric properties in the $BaTiO_3$/poly(vinylidene fluoride) nanocomposite films, *Appl. Phys. Lett.* **100** (2012) 012903.

[73] K. Li, H. Wang, F. Xiang, W. Liu, H. Yang, Surface functionalized $Ba_{0.6}Sr_{0.4}TiO_3$/poly(vinylidene fluoride) nanocomposites with significantly enhanced dielectric properties, *Appl. Phys. Lett.* **95** (2009) 202904.

[74] Z.-M. Dang, H.-Y. Wang, H.-P. Xu, Influence of silane coupling agent on morphology and dielectric property in $BaTiO_3$/polyvinylidene fluoride composites, *Appl. Phys. Lett.* **89** (2006) 112902.

[75] S. A. Paniagua, Y. Kim, K. Henry, R. Kumar, J. W. Perry, S. R. Marder, Surface-initiated polymerization from barium titanate nanoparticles for hybrid dielectric capacitors, *ACS Appl. Mater. Interfaces* **6** (2014) 3477-3482.

[76] L. Xie, X. Huang, Y. Huang, K. Yang, P. Jiang, Core-shell structured hyperbranched aromatic polyamide/$BaTiO_3$ hybrid filler for poly(vinylidene fluoride-trifluoroethylene-chlorofluoroethylene) nanocomposites with the dielectric constant comparable to that of percolative composites, *ACS Appl. Mater. Interfaces* **5** (2013) 1747-1756.

[77] W. Yang, S. Yu, R. Sun, R. Du, Nano- and microsize effect of CCTO fillers on the dielectric behavior of CCTO/PVDF composites, *Acta Mater.* **59** (2011) 5593-5602.

[78] Y. Yang, B.-P. Zhu, Z.-H. Lu, Z.-Y. Wang, C.-L. Fei, D. Yin, R. Xiong, J. Shi, Q.-G. Chi, Q.-Q. Lei, Polyimide/nanosized $CaCu_3Ti_4O_{12}$ functional hybrid films with high dielectric permittivity, *Appl. Phys. Lett.* **102** (2013) 042904.

[79] Z. M. Dang, J. B. Wu, L. Z. Fan, C. W. Nan, Dielectric behavior of Li and Ti co-doped NiO/PVDF composites, *Chem. Phys. Lett.* **376** (2003) 389-394.

[80] D. Bhadra, M. G. Masud, S. K. De, B. K. Chaudhuri, Large magnetoelectric effect and low-loss high relative permittivity in 0–3 CuO/PVDF composite films exhibiting unusual ferromagnetism at room temperature, *J. Phys. D: Appl. Phys.* **45** (2012) 485002.

[81] C. C. Wang, Y. M. Cui, L. W. Zhang, Dielectric properties of $TbMnO_3$ ceramics, *Appl. Phys. Lett.* **90** (2007) 012904.

[82] J. Li, F. Li, Y. Zhuang, L. Jin, L. Wang, X. Wei, Z. Xu, S. Zhang, Microstructure and dielectric properties of (Nb+In) co-doped rutile TiO_2 ceramics, *J. Appl. Phys.* **116** (2014) 074105.

[83] H. Zheng, W. Weng, G. Han, P. Du, Colossal permittivity and variable-range-hopping conduction of polarons in $Ni_{0.5}Zn_{0.5}Fe_2O_4$ Ceramic, *J. Phys. Chem. C* **117** (2013) 12966-12972.

[84] Y.-l. Su, C. Sun, W.-q. Zhang, H. Huang, Fabrication and dielectric properties of $Na_{0.5}Bi_{0.5}Cu_3Ti_4O_{12}$/poly(vinylidene fluoride) composites, *J. Mater. Sci.* **48** (2013) 8147-8152.

[85] T. B. Adams, D. C. Sinclair, A. R. West, Giant barrier layer capacitance effects in $CaCu_3Ti_4O_{12}$ ceramics, *Adv. Mater.* **14** (2002) 1321-1323.

[86] S. Maensiri, P. Thongbai, T. Yamwong, Giant dielectric response in (Li, Ti)-doped NiO ceramics synthesized by the polymerized complex method, *Acta Mater.* **55** (2007) 2851-2861.

[87] C. Wang, W. Ni, X. Sun, L. Wang, C. Wang, K. Jin, Relaxor-like behaviors in $Na_{1/2}Bi_{1/2}Cu_3Ti_4O_{12}$ ceramics, *J. Am. Ceram. Soc.* **100** (2017) 2016-2023.

[88] X. Zhu, L. Yang, J. Li, L. Jin, L. Wang, X. Wei, Z. Xu, F. Li, The dielectric properties for (Nb, In, B) co-doped rutile TiO_2 ceramics, *Ceram. Int.* **43** (2017) 6403-6409.

[89] X.-g. Zhao, P. Liu, Effects of sintering atmosphere on microstructure and dielectric properties of (Yb+Nb) co-doped rutile TiO_2 ceramics, *J. Alloys Compd.* **715** (2017) 170-175.

[90] X.-g. Zhao, P. Liu, Dielectric and electric relaxations induced by the complex defect clusters in (Yb+Nb) co-doped rutile TiO_2 ceramics, *J. Am. Ceram. Soc.* **100** (2017) 3505-3513.

[91] T. Adams, D. Sinclair, A. West, Characterization of grain boundary impedances in fine- and coarse-grained $CaCu_3Ti_4O_{12}$ ceramics, *Phys. Rev. B* **73** (2006) 094124.

[92] W. Li, R. Schwartz, Maxwell-Wagner relaxations and their contributions to the high permittivity of calcium copper titanate ceramics, *Phys. Rev. B* **75** (2007) 012104.

[93] P. Thongbai, J. Jumpatam, B. Putasaeng, T. Yamwong, S. Maensiri, The origin of giant dielectric relaxation and electrical responses of grains and grain boundaries of W-doped $CaCu_3Ti_4O_{12}$ ceramics, *J. Appl. Phys.* **112** (2012) 114115.

[94] Y. Song, X. Wang, Y. Sui, Z. Liu, Y. Zhang, H. Zhan, B. Song, Z. Liu, Z. Lv, L. Tao, J. Tang, Origin of colossal dielectric permittivity of rutile $Ti_{0.9}In_{0.05}Nb_{0.05}O_2$: Single crystal and polycrystalline, *Sci. Rep.* **6** (2016) 21478.

[95] M. Li, A. Feteira, D. C. Sinclair, Relaxor ferroelectric-like high effective permittivity in leaky dielectrics/oxide semiconductors induced by electrode effects: A case study of CuO ceramics, *J. Appl. Phys.* **105** (2009) 114109.

[96] J. Boonlakhorn, B. Putasaeng, P. Kidkhunthod, P. Thongbai, Improved dielectric properties of (Y+Mg) co-doped $CaCu_3Ti_4O_{12}$ ceramics by controlling geometric and intrinsic properties of grain boundaries, *Mater. Des.* **92** (2016) 494-498.

[97] Y. Cheng-Fu, An equivalent cicuit for CuO modified surface barrier layer capacitors, *Jpn. J. Appl. Phys.* **36** (1997) 188-193.

[98] C. C. Wang, L. W. Zhang, Surface-layer effect in $CaCu_3Ti_4O_{12}$, *Appl. Phys. Lett.* **88** (2006) 042906.
[99] P. Thongbai, T. Yamwong, S. Maensiri, Electrical responses in high permittivity dielectric (Li, Fe)-doped NiO ceramics, *Appl. Phys. Lett.* **94** (2009) 152905.
[100] S. Krohns, P. Lunkenheimer, S. G. Ebbinghaus, A. Loidl, Colossal dielectric constants in single-crystalline and ceramic $CaCu_3Ti_4O_{12}$ investigated by broadband dielectric spectroscopy, *J. Appl. Phys.* **103** (2008) 084107.
[101] R. D. Shannon, Revised effective ionic radii and systematic studies of interatomic distances in halides and chalcogenides, *Acta Crystallogr., Sect. A* **32** (1976) 751-767.
[102] T. B. Adams, D. C. Sinclair, A. R. West, Influence of processing conditions on the electrical properties of $CaCu_3Ti_4O_{12}$ ceramics, *J. Am. Ceram. Soc.* **89** (2006) 3129-3135.
[103] P. Ren, J. He, X. Wang, M. Sun, H. Zhang, G. Zhao, Colossal permittivity in niobium doped $BaTiO_3$ ceramics annealed in N_2, *Scr. Mater.* **146** (2018) 110-114.
[104] X. H. Wang, R. Z. Chen, Z. L. Gui, L. T. Li, The grain size effect on dielectric properties of $BaTiO_3$ based ceramics, *Mater. Sci. Eng. B* **99** (2003) 199-202.